NANOSYSTEMS:
PHYSICS, CHEMISTRY, MATHEMATICS

Polyakov E.V., Maksimova M.A., et al. *Nanosystems: Phys. Chem. Math.*, 2023, **14** (2), 231–241.
http://nanojournal.ifmo.ru
DOI 10.17586/2220-8054-2023-14-2-231-241

Original article

Colloidal-chemical mechanism of $Zn(OH)_2$–ZnO layer formation at the glass – ammonia solution – Zn(II) interface

Evgeny V. Polyakov, Maria A. Maksimova, Julia V. Kuznetsova, Larisa Yu. Buldakova

Institute of Solid State Chemistry of Ural Branch of Russian Academy of Sciences, Ekaterinburg, Russia

Corresponding author: Evgeny V. Polyakov, polyakov@ihim.uran.ru

PACS 81.15.-z

ABSTRACT Thermodynamic and experimental studies of $Zn(OH)_2$/ZnO particle formation conditions in the model of closed system Zn^{2+}–$NH_{3,aq}$–$NH_{3,gas}$–H^+–OH^-–H_2O–$N_{2,gas}$ (1), which often occurs in the process of synthesis of zinc oxide nanoparticles and films by chemical bath deposition (CBD) methods, were carried out. It was shown that the driving force for the formation and growth of $Zn(OH)_2$/ZnO particles in the initially homogeneous system (1) at 25 °C is the difference in the chemical potential of particles at the initial temperature (unsaturated system) and the synthesis temperature (supersaturated system). Using vibrational spectroscopy, X-ray phase and chemical analysis, diffuse light scattering and electrophoresis methods, it was found that the phase transformation of $Zn(OH)_2$ into ZnO takes place in the region of 85 – 90 °C. The colloid-chemical transformation of $Zn(NH_3)_4^{2+}$ ionic particles into colloidal polycrystals of $Zn(OH)_2$/ZnO composition was established for the first time to be a staged process. The first stage of the process in the solution volume is localized at the gas nanobubble-solution interface as a result of rapid formation, growth and removal of gas nanobubbles from the solution. The interaction of positively charged $Zn(OH)_2$ nanoparticles with the surface of larger negatively charged gas nanobubbles creates colloidal aggregates "bubble||surface film of hydroxide nanoparticles". Their adhesion forms an openwork foam-like structure of the colloid in the solution and in the film on the interfaces at the first stage of synthesis. After degassing of the electrolyte solution, the second stage develops, consisting of the nucleation and ionic-molecular growth of $Zn(OH)_2$/ZnO particles from the supersaturated solution, their distribution between the solution and the electrolyte – reactor wall – air interfaces. The film growth at this stage is regulated by the difference in surface charges of the double electric layer of the interface and polycrystalline colloidal particles. In the solution and on the interface, columnar $Zn(OH)_2$/ZnO structures grow as volumetric stars with conical hexagonal spikes.

KEYWORDS $Zn(OH)_2$, ZnO, layer, formation, glass, interface, mechanism, colloidal-chemical, NH_3 solution

ACKNOWLEDGEMENTS This study was performed in the framework of the state-financed topic AAAA-A19-119031890028-0 at ISSC UB RAS.

FOR CITATION Polyakov E.V., Maksimova M.A., Kuznetsova Yu.V., Buldakova L.Yu. Colloidal-chemical mechanism of $Zn(OH)_2$–ZnO layer formation at the glass – ammonia solution – Zn(II) interface. *Nanosystems: Phys. Chem. Math.*, 2023, **14** (2), 231–241.

1. Introduction

Colloidal-chemical synthesis of laminar systems (films, layers, coatings) from liquid phase, the systematic study of which began in the last century [1], has been developed in the last decade under the name of "chemical bath deposition" (CBD) methods [2–5]. Compared to physical methods, this is one of simple and relatively economical methods of creating films, layers, coatings on substrates, because it does not require expensive and special equipment, the use of high temperatures and high pressures, and is convenient for deposition on large-area substrates. This method can be used for producing thin films with controlled structure and morphology, such as nanocrystalline layers, nanowires and nanoribbons. CBD is used to make a variety of flat, spherical, porous films. The disadvantage of colloidal-chemical synthesis of films is its relatively low reproducibility compared to physical deposition methods. This limitation is eliminated by optimizing the growth parameters [6]. Among various chemical objects of film synthesis by CBD methods, the first place belongs to chalcogenide films [5, 7]. Along with them, of particular interest over the past decades was the production of 1D coatings, metallic nano-sized compounds, and semiconductors such as ZnO. Their synthesis makes it possible to create ultradisperse wires, wires and rods on inorganic and polymeric substrates for elements of solar converters, electronic circuits, radiation shields, and light concentrators [8–12].

In the general scheme of application of this method [2, 3] for obtaining Zn(II) oxide films, two groups can be distinguished. One of them is based on the spontaneous decomposition reactions of homogeneous alkaline solutions of zinc hydroxo-complexes [13, 14]. The other group assumes the use of alkaline ammonia solutions and additionally introduced

precursors based on organic ammonia derivatives (urea, hexamethylantetramine, mono-, di-, triethanolamine, dimethylamine, tetramethylammonium, etc.), the thermal decomposition of which at elevated temperatures and pressures leads to the release of ammonia into the solution and the formation of ammonia zinc complexes [15–17]. The use of organic ammonia derivatives and other organic components for the synthesis of oxide films associated with the release of ammonia gas into the air creates an additional load on the environment in the production of such functional materials [18].

The canonical method for the estimation of film synthesis parameters from an initially homogeneous solution at elevated temperatures is the thermodynamic analysis of the considered chemical system [4, 5]. The distribution diagrams of complex ions and calculation of solubility curves at different temperatures for predicting the region of ZnO film production in the system "$ZnCl_2$–NH_3–OH–H_2O – temperature" showed [19] that ZnO films can be obtained at solution pH above 7. The morphology of such films depends on the pH of the solution, the polycrystals of nanoparticles in the form of flowers or columnar structures growing in the area where $Zn(NH_3)_4^{2+}$ complexes predominate. In the region of pH>12, where $Zn(OH)_n^{2-n}$ ions dominate, nano-sized oxide flakes are formed. Solution temperature plays an important role in the morphology and equilibrium composition of oxide films. ZnO films deposited at high temperature (90 °C) have an oriented hexagonal structure (zincite) and [Zn]/[O] $\approx$ 1 stoichiometry, while at lower temperatures (70 °C) flaky amorphous films are formed. The main reaction that accompanies film growth is heterogeneous decomposition of ammonia or zinc hydroxo-complex in alkaline medium [19–21]. The cited papers note the thermodynamic probability of formation of ammonia molecules during decomposition of ammonia zinc complexes in an initially homogeneous solution, but the role of the gas phase in the growth mechanism of colloidal particles in solution and in the film is not considered. The presence of sulfide ions in the reaction bath does not exclude the formation of zinc oxide nanoparticles of a more complex composition [22]. According to X-ray photoelectron spectroscopy data, the oxide films grown in the region dominated by the ammonia complex are enriched with Zn(II) ions. The oxide growing in the region dominated by hydroxocomplexes contains Zn(II) vacancies in the metal sublattice [19]. The synthesis temperature also affects the ratio of the $Zn(OH)_2$/ZnO phases in the films and the optical bandgap of the solid phase. Luminescence intensity decreases when passing from $Zn(OH)_2$ to ZnO [23].

The application of thermodynamic modeling methods allows one to reveal the equilibrium characteristics and probable conditions of zinc oxide phase formation, but they do not establish the reasons for predominant phase release in the solution volume or in the interface region, the stages and mechanisms of colloidal-chemical transformations accompanying the processes of zinc complexes thermochemical decay in solution and the influence of system temperature on these processes.

Since numerous descriptions of conditions for producing chalcogenide and oxide films by the CBD method contain ammonia and ammonia zinc complexes as obligatory components, it was of interest to determine the general elements of the colloidal-chemical mechanism of formation and growth of nano-, microparticles of $Zn(OH)_2$/ZnO phases in the solution volume and on the "solution/reactor wall" interface during thermal action on the simplest in chemical respect model system

$$Zn^{2+} - NH_{3,aq} - NH_{3,gas} - H^+ - OH^- - H_2O - N_{2,gas} \quad (1)$$

as well as to find out the role of dissolved gas nano/micro-bubbles liberated in the solution volume in the mechanism of zinc oxide and zinc hydroxide formation depending on the temperature during the thermal action on (1).

2. Experimental

In order to establish the effect of chemical composition and temperature on the phase composition of products in a closed multiphase system (1), we used in this work the technique of thermodynamic analysis to quantify the chemical composition taking into account the following basic chemical components: NH_3(g), NH_3(a), O_2(g), N_2(g), H_2O(g), H_2O(a), H_2O(g), Zn(0), Zn(+2a), OH(–a), H(+a), $Zn(OH)_2$(ia), $ZnNH_3$(+2a), $Zn(NH_3)_2$(+2a), $Zn(NH_3)_3$(+2a), $Zn(NH_3)_4$(+2a), ZnOH(+a), $Zn(OH)_2$(0a), $Zn(OH)_3$(–a), $Zn(OH)_4$(–2a), ZnO, $Zn(OH)_2$. The dependences of the phase composition of system (1) were analyzed in pH–Eh, composition-temperature and composition-pressure coordinates using the HSC Chemistry 8 program. The "g" sign in the formulas refers to the gas phase, "a" – to the hydrated ions in solution, and the rest – to the liquid and solid phases.

Elemental analysis by inductively coupled plasma mass spectrometry (Elan 9000, [24]) was used to experimentally determine the kinetics of Zn(II) mass transfer during the transformation of a homogeneous zinc ammine solution into a colloidal $Zn(OH)_2$/ZnO solution in the aqueous phase and on the solution-glass substrate interface. The zinc salt solution for the kinetic experiment was prepared by dissolving 4.39 g of chemically pure zinc acetate $Zn(CH_3COO)_2 \cdot 2H_2O$ in 60 – 70 ml of deionized water (Millipore Simplicity system, solution resistance 18 MΩ·cm). Then 10 ml of concentrated ammonia was added to the solution and the pH of this solution was adjusted up to pH = 10.2 – 10.3 using a NaOH solution with a concentration of 0.05 M. After that the volume of the solution was brought up to 100 ml. In the kinetics experiments, 5 ml aliquots of the prepared solution were transferred sequentially with a glass pipette into glass test tubes. The test tubes were preliminarily chemically cleaned of traces of impurities by washing with concentrated hydrochloric acid and deionized water and then they were dried.

The experiments on the kinetics of spontaneous decomposition of a homogeneous ammonium solution of zinc ammine with isolation of $Zn(OH)_2$/ZnO established the regularities of changing of the concentration of Zn(II) in the form of colloid, filtrate and oxide/hydroxide film on a substrate depending on the isothermal heating time of the examined system (1) at a given temperature.

The colloidal part was separated by ultrafiltration through a double cellulose filter with a pore size of less than 100 nm under vacuum. The precipitate on the filter was dried at room temperature and dissolved in 2 mol/l hydrochloric acid (chemically pure grade) of a specified volume. Then we determined the mass of Zn in the volume and recalculated it in the mass (mol) of the metal in the form of colloid in (1) at a given time of synthesis. We also determined the mass of Zn in the filtrate after it was acidified to a concentration of 1.8 – 2.0 mol/l with hydrochloric acid directly in the test tube. The content of zinc, which formed a film on the walls of the quartz glass reactor, was determined after dissolving a layer with 2 mol/l hydrochloric acid with a volume equal to the volume of the studied solution, 5 ml. Along with chemical elemental analysis of $Zn(OH)_2$/ZnO formation in (1), layer formation was studied by Dynamic Light Scattering (DLS) and Laser Doppler Electrophoresis measurements carried out on a Zetasizer Nano ZS particle analyzer (Malvern Panalytical Ltd.) [24, 25].

The Raman spectral analysis of the samples was performed at room temperature using a Via Reflex Renishaw spectrometer ($\lambda = 532$ nm, $P = 25$ mW). The phase analysis of the products was fulfilled on a STADI-P X-ray powder automatic diffractometer (STOE) with CuKα1 radiation using the library of X-ray diffraction data PDF-2 (ICDD Release 2009). The morphology of the layers on the substrate was studied using the scanning electron microscopy (SEM) and EDX elemental analysis on a JSM JEOL 6390LA facility. The UV-visible absorption spectroscopy was performed using a Shimadzu UV-3101PC UV/Vis/Near-IR Spectrophotometer. The diffuse reflectance spectra of the layers were recorded in the interval of 220 – 800 nm by means of a Shimadzu UV-3600 UV-vis-NIR spectrophotometer using $BaSO_4$ crystals as a reference.

The measurement of the size and electrophoretic mobility of colloidal particles in dynamic light scattering and laser Doppler electrophoresis experiments had some special features. Since the transfer of the studied solution from the thermostat to the device cell did not make it possible to perform measurements in real time and temperature, the particle size was determined by heating and holding the examined system (1) directly in the Zetasizer Nano ZS cuvette. The result of the analysis of fluctuations of the Brownian motion velocity of particles was presented as the size of solvated particles (D, nm) by the Stokes–Einstein formula. The radiation source was a helium-neon laser with a wavelength of 633 nm. Measurements were taken in a glass cuvette at temperatures in the range of 25 – 60 °C at a scattering angle of 173 ° (backscattering), Fig. 1. In addition to the diffusion parameters, the device measured the electrical conductivity of the solution (Q) and the intensity of the backscattered photon flux. This made it possible to obtain D values taking into account the attenuation of the light flux as it passes through the cuvette wall and the constantly changing colloidal solution. The changes in the relative concentration of Zn(II) in the form of colloid (precipitate), filtrate (solute) and film of oxide/hydroxide on the substrate, as well as in the average hydrodynamic diameter of colloid particles D, their zeta potential and solution conductivity Q with the time of synthesis are shown as an example in Fig. 2.

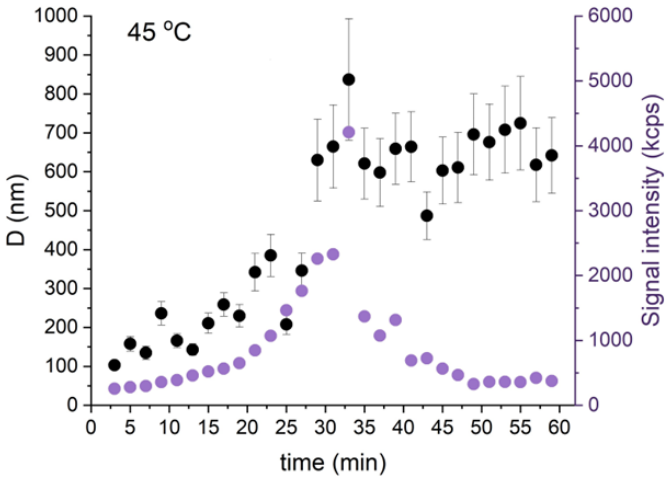

FIG. 1. Signal intensity (violet points) and mean hydrodynamic diameter (D, black points) of $Zn(OH)_2$/ZnO particles formed at 45 °C according to direct measurements. Confidence intervals characterize the scattering in the size distribution of the hydrodynamic diameter of growing particles at each time point

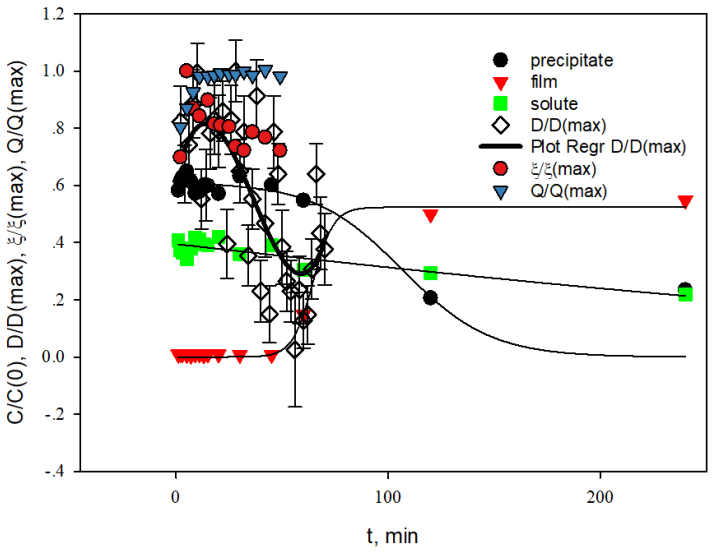

FIG. 2. Example of changes in the relative concentration of Zn(II), $C/C(0)$ in the form of colloid, film and ions, in NH_3–Zn(II) solution; changes in colloid particle size, $D/D_{\max}$, according to light scattering data ($D_{\max} = 400$ nm); changes in the relative conductivity $Q/Q_{\max}$ and the particle zeta potential $\xi/\xi_{\max}$ with the synthesis time t. C, $C(0)$ are the current and initial concentration of Zn(II) in the phase. The maximal zeta potential, $\xi_{\max} = +21.6$ mV; Q is the electrical conductivity; $Q_{\max} = 27.1$ mS/sm; temperature 55 °C, pH = 10.3

3. Experiment results

The thermodynamic study of the elements of the growth mechanism of $Zn(OH)_2$ – ZnO layers on the glass surface was performed in the model system Zn^{2+} – $NH_{3,aq}$ – NH_3(g) – OH^- – H_2O – N(g) (1). Here, hydrated ammonia molecules $NH_{3,aq}$ in the selected pH range simultaneously acted as a ligand and a film-forming agent. The fields of predominance of ionic particles and $Zn(OH)_2$ – ZnO – Zn(0) phases in Eh–pH coordinates, where Eh(B) is the electrochemical potential (1) relative to the hydrogen electrode for temperatures 25 and 85 °C, are shown in Fig. 3. From the data of thermodynamic calculation it is evident that the appearance of the solid phase in (1) when the temperature changes from 25 to 85 °C in the pH range 8.6 – 10.8 is caused by the formation of oversaturated solution relative to zinc hydroxide (< 35 °C) or oxide (> 40 °C) due to the system exit from the $Zn(NH_3)_4^{+2}$ complex stability field in this pH region. The simultaneous effect of pH and temperature of system (1) on the chemical and phase composition of zinc compounds according to the calculation data is illustrated in Fig. 4. It is seen that at 25 – 35 °C and pH < 10.3 the ammonia solution of Zn(II) is not saturated relative to the oxide or hydroxide. The main chemical form of ions in the solution is the $Zn(NH_3)_4^{+2}$ complex. Note that $Zn(NH_3)_4^{+2}$ is a cationic component of the complex whose stability is determined in the HSC Chemistry 8 database. It is obvious that in the examined pH region, ammonia complexes can exist in the form of ionic pairs with hydroxyl ions or mixed ligand hydroxo-complexes. There is no information in the thermodynamic literature on the existence and stability of mixed hydroxo-ammonium zinc complexes. It is known that for mixed ligand metal complexes MX, MY, the logarithm of the stability constant is $\log(\beta_{MXY}) \approx \frac{1}{2}(\log(\beta_{MX}) + \log(\beta_{MY}))$ [26]. For $Zn(NH_3)_4(OH)^+$, this estimation gives one $\log(\beta_{MXY}) \approx 6.9$, which is 2 log units less than $\log(\beta MY)$ of $Zn(NH_3)_4^{2+}$ complex [27]. This estimate shows that ammonia complexes are most likely to exist in alkaline solution mainly in the form of ionic pairs with OH-ions. From Figs. 4 and 5, it follows that the temperature increase in the equilibrium model system (1) at the zinc concentration 0.06 mol/l keeps it homogeneous in the pH interval 10.0 – 10.5 up to a temperature of 35 °C. With a further increase in pH in this temperature range, system (1) transits to a supersaturated solution state with a release of a mixture of ε-$Zn(OH)_2$ – ZnO phases. Simultaneously, the partial pressure of ammonia in the gas phase NH_3(g) increases, but the concentration of dissolved ammonia changes little if at all, Fig. 3. The transfer of NH_3(g) into the gas phase takes place from the electrolyte surface, as well as by the formation, growth in the electrolyte volume, and removal to the electrolyte surface of nano- and micro-bubbles of dissolved gases, primarily H_2O(g) and NH_3(g) [28].

According to the X-ray phase analysis of precipitates and films on the reactor surface, the observed picture of phase transformations in system (1) is different from the data of thermodynamic calculations in that the phase transition takes place in the region of higher temperatures, Figs. 6, 7(a).

The appearance of the ZnO phase (wurtzite) is observed at 95 – 99 °C. Independent results of Raman spectroscopy of films in the region of deformation vibration bands of hydroxide OH-groups (3190 and 3266 1/cm [29]) obtained at different temperatures of system (1) illustrate the gradual disappearance of the zinc hydroxide phase, Fig. 7(a). The

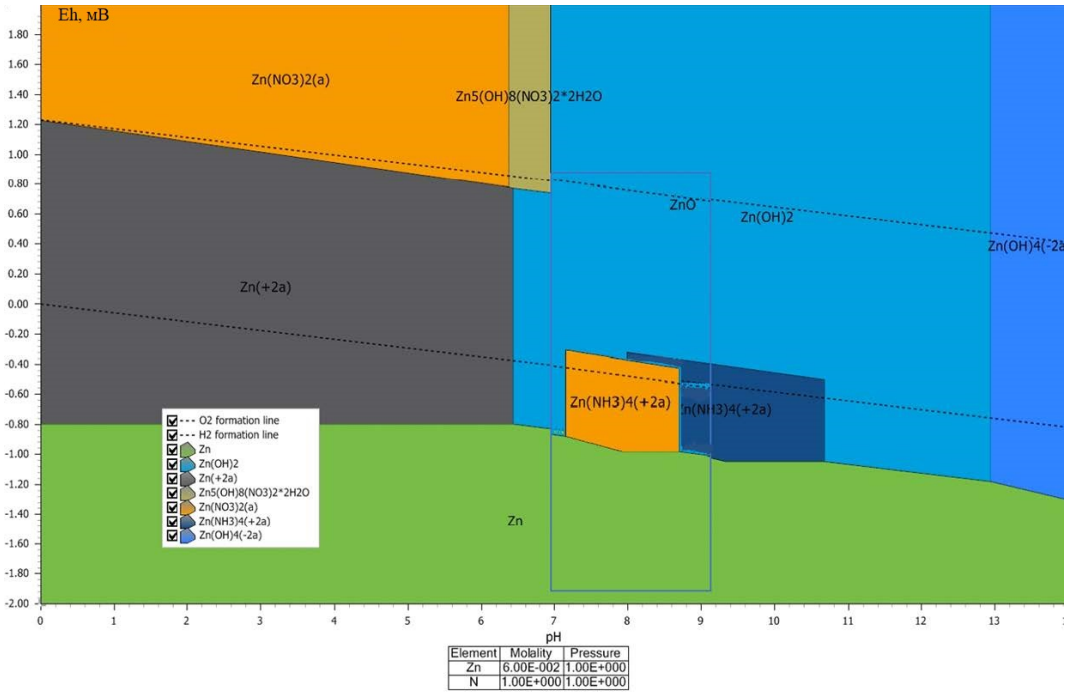

FIG. 3. Pourbaix diagram calculated for system (1) using the HSC Chemistry 8 program. The concentration of Zn(II) is 0.06 mol/l, the concentration of ammonia in solution is 1 mol/l, the total pressure of N_2–O_2–H_2O(g) gas mixture in the system is 1 atm, 22 °C. Eh is the electrochemical potential in the system relative to the hydrogen electrode, B. The dark blue area shows the field of predominance of the $Zn(NH_3)_4^{+2}$ complex. The inset in the blue frame shows the field of predominance (orange color) of the $Zn(NH_3)_4^{+2}$ complex at 85 °C in the same pH range.

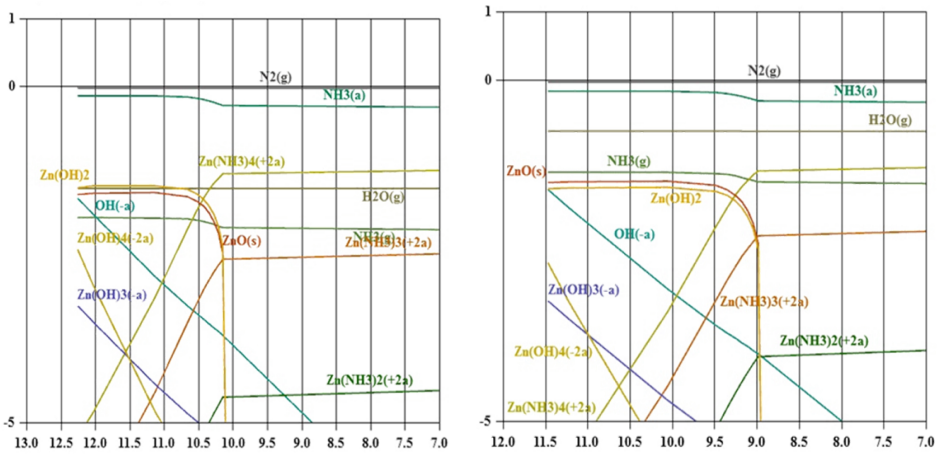

(a) (b)

FIG. 4. Changes in the chemical and phase composition in system (1) as a function of pH and temperature; the concentration of Zn(II) is 0.06 mol/l, the concentration of ammonia in solution is 1 mol/l, the total pressure of N_2–O_2–H_2O(g) gas mixture in the system is 1 atm.

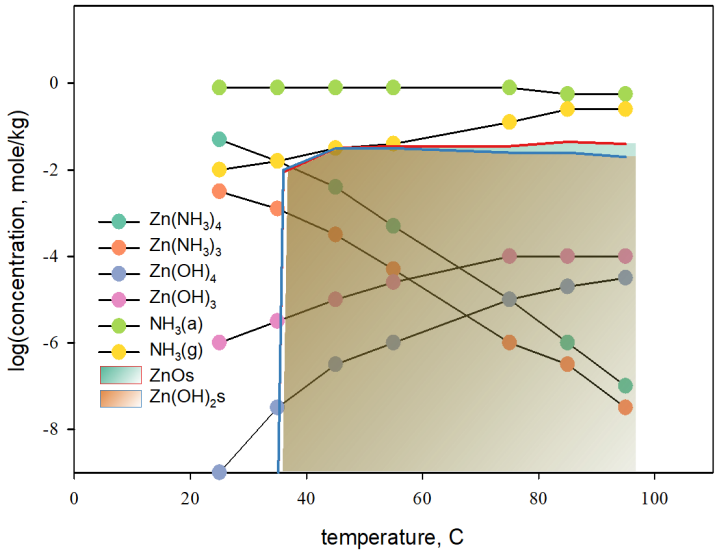

FIG. 5. The calculation results of the changes in the chemical and phase composition of the solution during synthesis as a function of temperature. The concentration of Zn = 0.06 mol/kg, NH_3 = 1 mol/kg, pH = 10.0 – 10.3. HSC Chemistry 8 program. (s) denotes the belonging to solid phase.

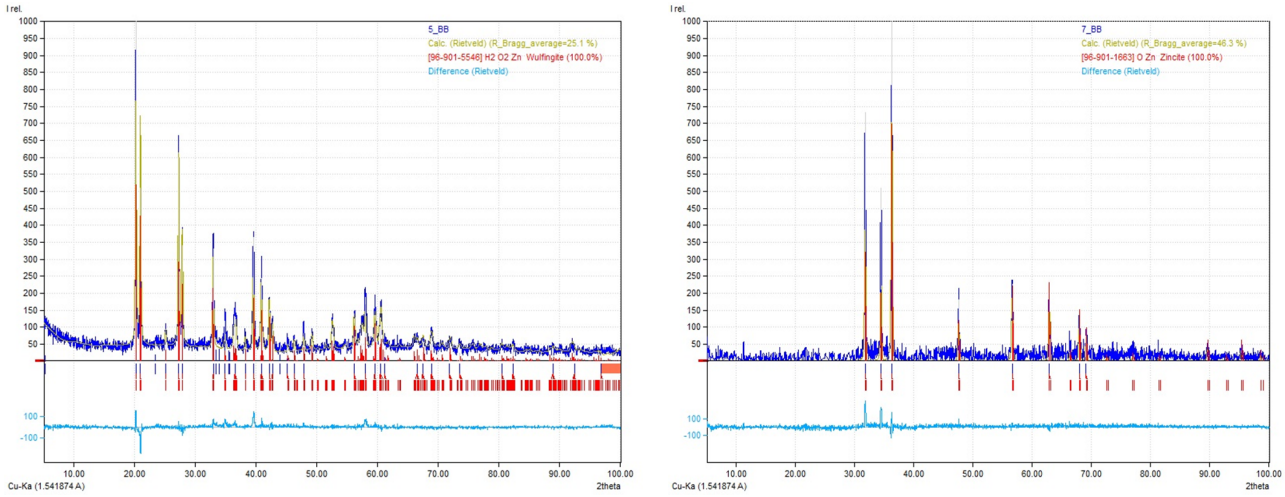

(a) (b)

FIG. 6. X-ray diffraction pattern of ε-$Zn(OH)_2$ (a) and ZnO (b) films deposited from the zinc ammonia solution on the glass surface. The film composition at (a) 80 °C – ε-$Zn(OH)_2$, (wulfingite) space group P 2_1 2_1 2_1, CSR (coherent scattering region) – 64 nm, at (b) 99 °C – ZnO, (wurtzite) space group P 6_3 m c, CSR – 71 nm. Dark blue line is the experimental data (1); yellow line is the result of description by the Rietveld method (2); red line is the tabulated values of phase intensities (3); light blue line is the difference between (1) and (2). Solution composition – Zn(II) = 0.12 mol/l, NH_3 = 1 mol/l, pH = 10.3.

change in the phase composition of the films, Figs. 6, 7, agrees with the literature data on the variation of the optical bandgap of the films obtained under the same conditions at different temperatures [20].

Measurements of the average hydrodynamic diameter of colloidal particles during synthesis at different temperatures showed that the precipitation of the solid phase in the form of a film on the electrolyte/reactor wall interface prevents the application of the dynamic light scattering method at temperatures above 55 °C. Typical dependence of the flux of detector-recorded photons backscattered on colloidal particles (Fig. 1) shows that the signal intensity passes through a maximum as the colloid forms, whereupon it decreases to background values due to their absorption by the $Zn(OH)_2$ film growing on the cuvette walls. At a temperature of 60 °C or higher, the film on the cuvette wall completely absorbs the photon flux already in the first minutes of the measurement. Therefore, we limited the temperature range of the study of colloidal properties of system (1) to 25 – 55 °C.

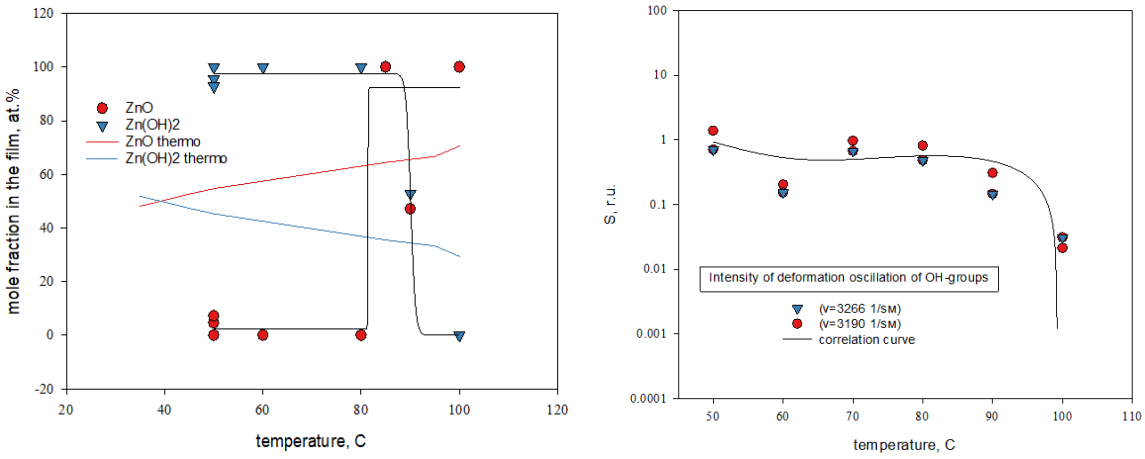

(a) (b)

FIG. 7. (a) Changes in the phase composition of the ZnO/$Zn(OH)_2$ film depending on the synthesis temperature. Dots – experiment, lines – thermodynamic calculation of the equilibrium composition. (b) Variation of the intensity (S) of deformation vibration bands of -OH groups in ε-$Zn(OH)_2$ (wulfingite) films on the glass surface with the synthesis temperature according to Raman spectroscopy data. S is the integrated intensity of signal in the absorption band (ν) region of the Raman spectrum. The line is the correlation curve "$\log(S)$–temperature".

According to the diffusion scattering measurements as a function of synthesis time, colloidal particles with an average size of 200 – 1000 nm, Fig. 8, and a positive value of ζ-potential, Fig. 9, are observed in system (1) at 25 °C and at elevated temperatures immediately after the preparation of the initial solution. At the same time, the solution looks optically transparent. The size of fixed particles (D) changes with synthesis time, regression line ($D/D_{\max}$), Fig. 2. Their ζ-potential first increases to the maximum value, then it decreases and further increases following the trend in the relative concentration $C/C(0)$ of zinc in the form of a film, Fig. 2.

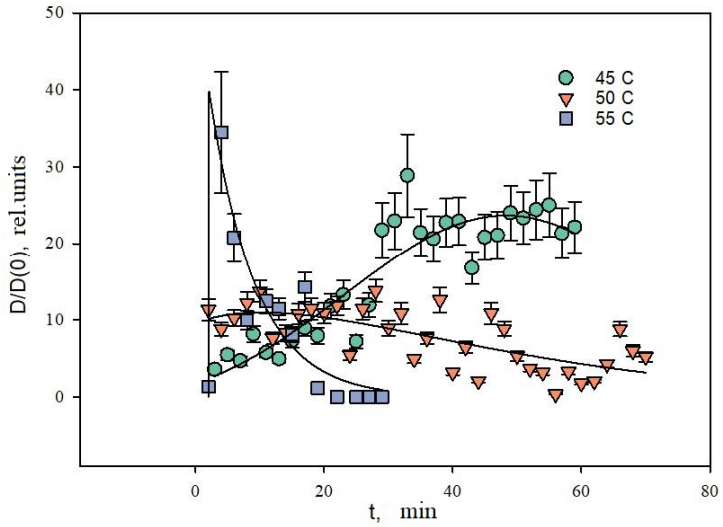

FIG. 8. Variation in the relative size $D/D(0)$ of ZnO/$Zn(OH)_2$ microcrystals in the film at synthesis temperatures 45, 50 and 55 °C with contact time. $D(0)$ is the value of the coherent scattering region of crystals calculated from phase analysis data (Debye–Scherrer equation). $D(0) = 29 \pm 5$ nm. The concentration of Zn(II) = 0.12 mol/l, NH_3 = 1 mol/l, pH = 10.3.

Two stages can be distinguished in the character of changes in the particle size D, Fig. 8, and ζ-potential, Fig. 9, with time at different synthesis temperatures. At the first stage, the main factor of the change (1) is the growth of conductivity (Q) of electrolyte solution, which is determined by thermal decay of $Zn(NH_3)_4^{2+}$ complex and hydrolysis of

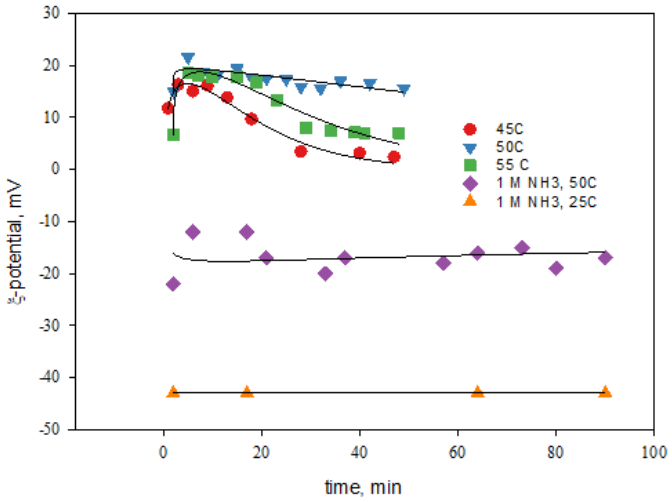

FIG. 9. Changes of ζ-potential of $Zn(OH)_2$/ZnO microcrystals with synthesis time during their growth from ammonia solution at different temperatures. The graph of behavior of ζ-potential of gas nanobubbles in ammonia solution without Zn(II) at 25 and 50 °C is given for comparison. Solution composition: Zn(II) = 0.12 mol/l, NH_3 = 1 mol/l, pH = 10.3.

ammonia molecules in solution according to the following reactions

$$\begin{aligned} Zn(NH_3)_4(OH)_2 &\rightarrow Zn^{2+}_{aq} + 4NH_{3,aq} + 2OH^-, \\ Zn^{2+}_{aq} + 2OH^- &\rightarrow Zn(OH)_{2,colloid}, \\ NH_{3,aq} + OH^- &\rightarrow NH_4OH \rightarrow NH^+_4 + OH^-. \end{aligned} \tag{2}$$

Destruction of $Zn(NH_3)_4(OH)_2$ ion pair leads to supersaturation with isolation of Zn(II) in the form of $Zn(OH)_2$ colloid and increases the concentration of ammonium ions in solution by reaction (2) and conductivity $Q(t)$, Fig. 10(a). The empirical relationship $Q(t) - t$ is described by the first order irreversible reaction equation throughout the temperature range 45 – 55 °C, Fig. 10(a):

$$Q(t) = a + b(1 - \exp(-ct)), \quad P(t) = (1 - (Q(t) - a)/b), \tag{3}$$

where a, b, c are equation parameters and $P(t)$ is an auxiliary function. Comparison of the conductivity in (1) with that of the ammonia solution at pH 10.3, Fig. 10(a), shows that ionic reactions (2) are completed by the accumulation of ammonium ions in solution during the first 10 to 15 minutes of synthesis. At the first stage, colloidal particles $Zn(OH)_2$ have a ζ-potential of approximately +(20 – 25) mV, which is typical of aqueous colloidal solutions of $Zn(OH)_2$, ZnO in the pH range 10 – 11 [6, 30]. The relatively large positive ζ-potential prevents the aggregation (increase in size) of particles and their attachment to interfaces, which explains the appearance of the induction period of film growth in $C/C(0) - t$ coordinates, Fig. 2. Even before the process of colloid formation in (1) begins, the appearance of nanoparticles identical to gas nanobubbles is noted in the homogeneous solution at 25 °C, Fig. 9 [28, 31, 32]. Their ζ-potential at pH 10.3 and 25 °C is negative, -40 mV, and increases to $-(15 – 20)$ mV when the temperature rises to 50 °C. This sign of the charge is characteristic of the gas nanobubbles in alkaline environment and is opposite to the sign of the ζ-potential of hydroxide colloid, Fig. 9. The presence of nano- (< 200 nm) and microbubbles (10 – 50 μm) of gas with negative zeta potential is typical for aqueous solutions of urea, ethanol, ammonia solutions, etc. Gas bubbles evolve over time, increasing in size and collapsing to form high-pressure microzones near the electrolyte-gas interface [32, 33].

The joint formation of colloidal particles and nanobubbles of gas in system (1) leads to their electrostatic attraction with a change in charge, size and morphology [34]. The interaction of gas nanobubbles and colloidal particles explains the stabilization and relatively large size of the observed colloidal particles due to adsorption of smaller positively charged $Zn(OH)_2$ nanoparticles on the surface of larger negatively charged gas nanobubbles and formation of colloidal aggregates "bubble||surface film of hydroxide nanoparticles" [34, 35]. Their further cohesion forms an openwork foamy colloid structure of solution and film on the solution/wall interface at the first stage of synthesis, Figs. 8, 11(a). The interaction of nanobubbles of gas and colloidal particles explains the large size of the observed colloidal particles, which is reflected in the morphology of films obtained under similar conditions, but annealed at 400 °C [36], Fig. 11(a).

At higher temperatures, the growth rate of the number and size of gas bubbles in (1) increases leading to their mass-transfer to the solute/gas interface and final removal from the solution [32, 33]. This allows us to suggest the following explanation for the change in the position of the maximum of the peak of the observed colloidal particle size distribution with temperature, Fig. 8. As the temperature increases, the time necessary to reach a maximum in the size distribution of the observed colloidal particles decreases, and at 55 °C the formation and then disappearance of large

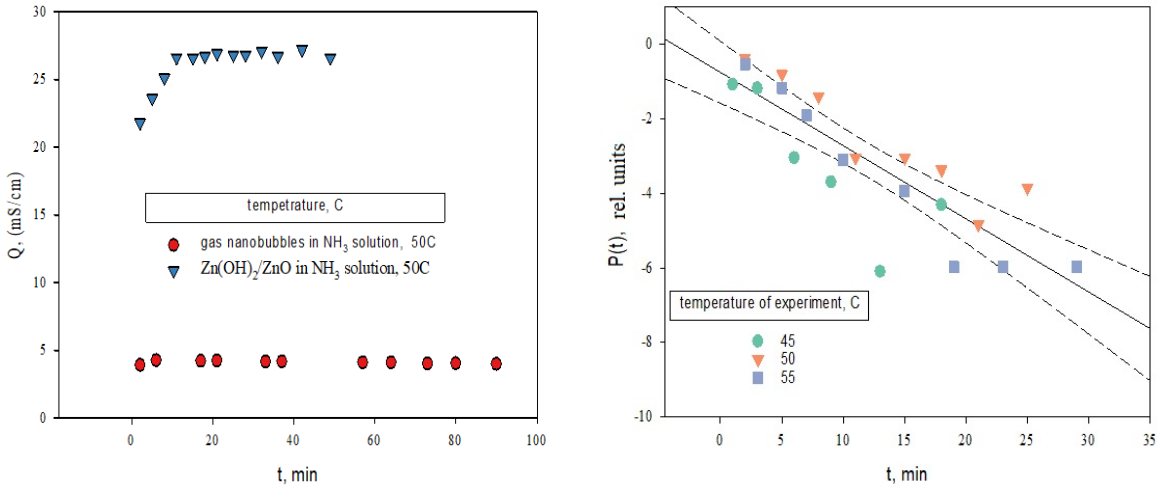

(a) (b)

FIG. 10. (a) Variation of the conductivity (Q) of colloidal solution $Zn(OH)_2$ (triangles) in system (1) and ammonia solution without addition of Zn(II) ions (circles) with time, 50 °C, pH 10.3. (b) Variation of the conductivity of solutions as a function of $Zn(OH)_2$ synthesis temperature, coordinates of eq. (3).

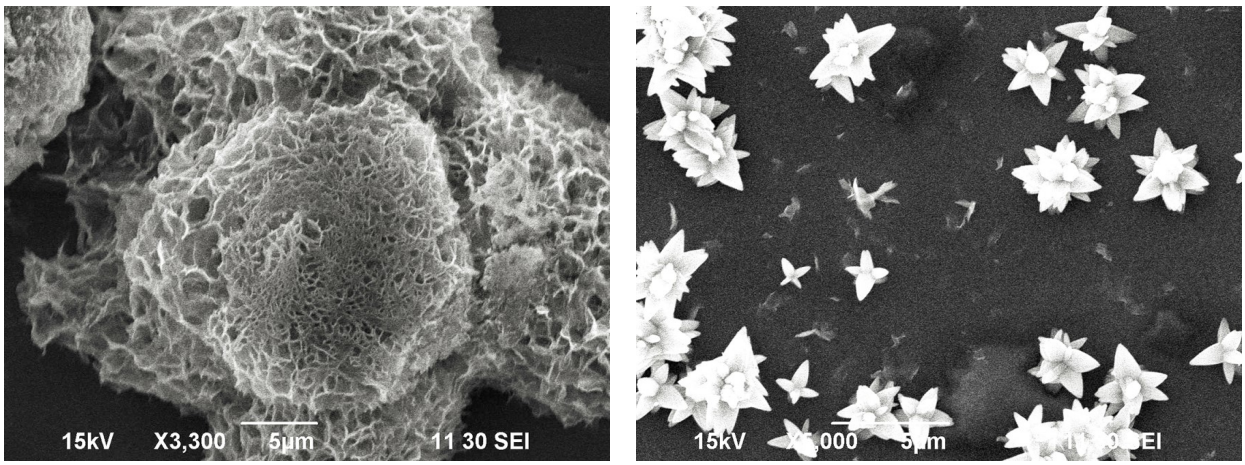

(a) (b)

FIG. 11. Microphotographs of films (a) – $Zn(OH)_2$, (b) – ZnO obtained after 5 minutes of synthesis at temperatures 50 °C (a), 90 °C (b)

colloidal particles and degassing of the solution occur in the first 1 – 2 minutes, Fig. 8. At the final stage of degassing of the solution, the colloidal aggregates of hydroxide nanoparticles on the surface of growing gas bubbles disintegrate, hydroxide nanoparticles that were formerly on their surface again pass to a state of bulk colloid, and the observed size of colloidal particles and their charge decrease, Fig. 9. Due to the removal of gas nanobubbles, the formation of openwork colloidal structures in the degassed solution (at elevated temperatures) becomes impossible. The same result should be achieved when the total pressure in the system increases, preventing the formation of gas bubbles in the electrolyte solution.

As the temperature rises, the second stage of the colloid formation process, which is a sequence of nucleation and ion-molecular growth reactions of $Zn(OH)_2$/ZnO nanoparticles in a degassed supersaturated solution volume and their heterogeneous distribution on the interfaces, becomes the main one, Fig. 2. The morphology of growing $Zn(OH)_2$ – ZnO crystallites at the second stage is determined by the conditions of their spontaneous crystallization and therefore differs greatly from the morphology of particles growing at the first stage on the surface of nanobubbles, Fig. 11(a,b). The driving force of the $Zn(OH)_2$/ZnO film growth on the reactor wall surfaces and the solution/air boundary is the difference in the electrochemical potentials of the double electric layer surface of the interfaces and nano-microcrystals. The morphology of crystallites at the second stage represents columnar structures and volumetric stars with spikes of hexagonal section

and conical shape, which is connected with their growth on lateral hexagonal faces of primary particles in conditions of gradual diminution of supersaturation [13–21].

4. Conclusion

The performed study of the equilibrium and dynamic conditions of $Zn(OH)_2$/ZnO nanoparticle formation in the model closed system Zn^{2+} – $NH_{3,aq}$ – NH_3(g) – OH^- – H_2O – N_2(g) (1) revealed that the driving force for the formation and growth of nanoparticles in the initially homogeneous system (1) at 25 °C is the difference in the chemical potential of particles at 25 °C (unsaturated system relative to $Zn(OH)_2$/ZnO formation) and a given synthesis temperature (supersaturated system). Using vibrational spectroscopy, X-ray phase and chemical analysis, diffuse light scattering and electrophoresis methods, it was found that the phase transformation of $Zn(OH)_2$ into ZnO occurs in the region of 85 – 90 °C, in contrast to the temperature of 35 – 40 °C according to thermodynamic simulation data. Changes in the relative concentration of Zn(II) in the form of colloid, the film and the ions in electrolyte solution and the electrical conductivity of the electrolyte solution with the time of synthesis corresponds to the first order reaction for ions Zn(II).

It has been shown for the first time that the colloidal-chemical transformation of $Zn(NH_3)_4^{2+}$ ionic particles into colloidal microcrystals of $Zn(OH)_2$ /ZnO composition is a staged process. The first stage of the process takes place in the solution volume mainly on the gas nanobubble-solution interfaces as a result of rapid formation, growth, and removal of gas nanobubbles from the solution. The driving force of the process at the first stage is the difference in the sign of the surface charges of nanobubbles and Zn(II) colloidal particles in the electrolyte volume. The interaction of small positively charged $Zn(OH)_2$ nanoparticles with the surface of larger negatively charged gas nanobubbles creates colloidal aggregates "surface film of hydroxide nanoparticles ||gas bubble". Their further cohesion leads to the formation of an openwork foamy structure of the colloid in solution and films on the interfaces at the first stage of synthesis. After degassing of the electrolyte solution, the second stage develops, which consists in nucleation and ionic-molecular growth of $Zn(OH)_2$/ZnO particles in the volume of the degassed supersaturated solution and in their distribution between the colloidal solution and "electrolyte – reactor wall – air" interfaces. In the absence of gas nanobubbles, columnar structures grow in the solution and at the interface in the form of volumetric stars with spikes of conical shape and hexagonal cross-section.

References

[1] Mokrushin S.G. Experimental study of laminar systems. *J. of Physical Chemistry*, 1934, **5** (8), P. 1082–1091.

[2] Fabian I.E., Chandrakant D.L., Rajan J. *Chemically Deposited Nanocrystalline Metal Oxide Thin Films: Synthesis, Characterizations, and Applications*. Springer Cham, 2021, 926 p.

[3] Guire M.R.D., Bauermann L.P., Parikh H., Bill J. Chemical Bath Deposition. In *Chemical Solution Deposition of Functional Oxide Thin Films*. Ed. Waser R., Kosec M., Payne D. Schneller T. Vienna, Springer, 2013.

[4] Markov V.F., Maskaeva L.N., Kitaev G.A. Peculiarites of microstructure and properties of lead sulfide films deposited from halide-containing solutions. *Inorganic materials*, 2000, **36** (7), P. 792–795.

[5] Kozhevnikova N.S., Markov V.F., Maskaeva L.N. Chemical deposition of metal sulfides from aqueous solutions: from thin films to colloidal particles. *J. of Physical Chemistry*, 2020, **94** (12), P. 1752–1766.

[6] Fatehah M.O., Hamidi A.A., Serge S. Stability of ZnO nanoparticles in solution. Influence of pH, dissolution, aggregation and disaggregation effects. *J. of Colloid Science and Biotechnology*, 2014, **3** (1), P. 75–84.

[7] Majid A., Bibi M. Cadmium based II-VI Semiconducting Nanomaterials Wet Chemical Synthesis Methods. *Topics in Mining, Metallurgy and Materials Engineering*, Springer, Cham, 2018, P. 43–101.

[8] Guillemin S., Rapenne L., Roussel H., Sarigiannidou E., Brémond G., Consonni V. Formation Mechanisms of ZnO Nanowires: The Crucial Role of Crystal Orientation and Polarity. *J. of Physical Chemistry C*, 2013, **117** (40), P. 20738–20745.

[9] He J.H., Lao C.S., Chen L.J., Davidovic D., Wang Z.L. Large-scale Ni-doped ZnO nanowire arrays and electrical and optical properties. *J. of the American Chemical Society*, 2005, **127** (47), P. 16376–16377.

[10] Comini E., Faglia G., Sberveglieri G., Pan Z.W., Wang Z.L. Stable and high-sensitive gas sensors based on semoconducting oxide nanobelts. *Applied Physics Letters*, 2002, **81** (10), P. 1869–1871.

[11] He J.H., Hsin C.L., Liu J., Chen L.J., Wang Z.L. Piezoelectric gated diode of a single ZnO nanowire. *Advanced Materials*, 2007, **19** (6), P. 781–784.

[12] Sun X., Li Q., Jiang J., Mao Y. Morphology-tunable synthesis of ZnO nanoforest and its photoelectrochemical performance. *Nanoscale*, 2014, **6** (15), P. 8769–8780.

[13] Pérez-Hernández R., Velázquez Salazar J.J., Yacaman M.J. Low-Temperature Synthesis and Growth Mechanism of ZnO Nanorods on Crystalline Si Substrate. *J. of Nano Research*, 2011, **14**, P. 69–82.

[14] Wang M., Jiang L., Jung Kim E., Hahn S.H. Electronic structure and optical properties of $Zn(OH)_2$: LDA+U calculations and intense yellow luminescence. *RSC Advances*, 2015, **5** (106), P. 87496–87503.

[15] Alnoor H., Chey Ch.O., Pozina G., Liu X., Khranovskyy V., Willander M., Nur O. Effect of precursor solutions stirring on deep level defects concentration and spatial distribution in low temperature aqueous chemical synthesis of zinc oxide nanorods. *AIP Advances*, 2015, **5**, 087180.

[16] Baviskar P.K., Nikam P.R., Gargote S.S., Ennaoui A., Sankapal B.R. Controlled synthesis of ZnO nanostructures with assorted morphologies via simple solution chemistry. *J. of Alloys and Compounds*, 2013, **551**, P. 233–242.

[17] Znaidi L. Sol-gel-deposited ZnO thin films: A review. *Materials Science and Engineering B*, 2010, **174**, P. 18–30.

[18] Le Pivert M., Martin N., Leprince-Wang Y. Hydrothermally grown ZnO nanostructures for water purification via photocatalysis. *Crystals*, 2022, **12** (3), 308.

[19] Gonzalez-Chan I.J., Moguel Z.P., Oliva A.I. Deposition of ZnO thin films by chemical bath technique: physicochemical conditions and characterization. *ECS J. of Solid State Science and Technology*, 2019, **8** (9), P. 536–544.

[20] Kahraman S., Çakmak H.M., Çetinkaya S., Çetinkara H.A., Güder H.S. CBD grown ZnO nanostructures: effects of solution temperature. *Int. J. of Materials Research*, 2013, **104** (8), P. 798–804.

[21] Trejo-Ramos A.I., Martín-Varguez P.E., Gonzalez-Chan I.J., Oliva A.I. Algorithm to obtain the species distribution diagrams and solubility curves for depositing ZnS, ZnO, and $Zn(OH)_2$ films in aqueous solution. *Computational and Theoretical Chemistry*, 2021, **1202**, 113325.
[22] Stefan M., Nistor S.V., Ghica D. ZnS and ZnO Semiconductor Nanoparticles Doped with Mn^{2+} Ions. Size Effects Investigated by EPR Spectroscopy. *Springer Series in Materials Science*, 2014, **205**, P. 3–27.
[23] Molefe F. V., Koao L. F., Dejene B. F., Swart H. C. Phase formation of hexagonal wurtzite ZnO through decomposition of $Zn(OH)_2$ at various growth temperatures using CBD method. *Optical Materials.* 2015, **46**, 292-298.
[24] Polyakov E.V., Tzukanov R.R., Volkov I.V., Buldakova L.Yu., Baklanova I.V., Lipina O.A., Zhukov V.P., Kuznetsova Yu.V., Tutyunnik A.P., Maximova M.A. Synthesis and comparative photocatalytic activity of CuO layers on SiO_2 substrates. *Nanosystems: Physics, Chemistry, Mathematics*, 2020, **11** (5), P. 601–607.
[25] Polyakov E.V., Tsukanov R.R., Buldakova L.Yu., Kuznetsova Yu.V., Volkov I.V., Zhukov V.P., Maksimova M.A., Dmitriev A.V., Baklanova I.V., Lipina O.A., Tyutyunnik A.P. Chemical Bath Precipitation and Properties of β-$Ni(OH)_2$ Films Prepared in Aqueous Ammoniac Solutions. *Russian J. of Inorganic Chemistry*, 2022, **67** (6), P. 912–920.
[26] Vasiliev V.P. *Thermodynamic properties of electrolyte solutions*. Vysshaya Shkola, 1982, 320 p.
[27] Kotrly S., Suka L. *Handbook on chemical equilibriq in analytical chemistry*. Ellis Horwood Limiòed, Chichester, 1985, 253 p.
[28] Margulis M.A. Sonoluminescence. *Uspekhi Fizicheskih Nauk*, 2000, **170** (3), P. 263–287.
[29] Lutz H.D, Jung C., Mörtel R., Jacobs H., Stahl R. Hydrogen bonding in solid hydroxides with strongly polarising metal ions, b-$Be(OH)_2$ and o-$Zn(OH)_2$. *Spectrochimica Acta Part A*, 1998, **54**, P. 893–901.
[30] Kim K.M., Kim T.H., Kim H.M., Kim H.J., Gwak G.H., Peak S.M., Oh J.M. Colloidal behaviors of ZnO nanoparticles in various aqueous media. *Toxicology and Environmental Health Sciences*, 2012, **4** (2), P. 121–131.
[31] Zhang X., Wang Q., Wu Zh., Tao D. An experimental study on size distribution and zeta potential of bulk cavitation nanobubbles. *Int. J. of Minerals, Metallurgy and Materials*, 2020, **27** (2), P. 152–161.
[32] Li M., Tonggu L., Zhan X., Mega T.L., Wang L. Cryo-EM Visualization of Nanobubbles in Aqueous Solutions. *Langmuir*, 2016, **32** (43), P. 11111–11115 .
[33] Agarwal A., Ng W.J., Liu Y. Principle and applications of microbubble and nanobubble technology for water treatment. *Chemosphere*, 2011, **84** (9), P. 1175–1180.
[34] Alheshibri M., Baroot A.A., Shui L., Zhang M. Nanobubbles and nanoparticles. *Current Opinion in Colloid & Interface Science*, 2021, **55** (43), 101470.
[35] Bui T.T., Nguyen D.C., Han M. Average size and zeta potential of nanobubbles in different reagent solutions. *J. of Nanoparticle Research*, 2019, **21** (8), P. 1–11.
[36] Pawar S.M., Gurav K.V., Shin S.W., Choi D.S., Kim I.K., Lokhande C.D., Rhee J.I., Kim J.H. Effect of bath temperature on the properties of nanocrystalline ZnO thin films. *J. of Nanoscience and Nanotechnology*, 2010, **10** (5), P. 3412–3415.

Submitted 16 December 2022; revised 6 March 2023; accepted 7 March 2023

Information about the authors:

Evgeny V. Polyakov – Institute of Solid State Chemistry of Ural Branch of Russian Academy of Sciences, 91, Pervomaiskaya str., 620108, Ekaterinburg, Russia; ORCID 0000-0001-7432-994X; polyakov@ihim.uran.ru

Maria A. Maksimova – Institute of Solid State Chemistry of Ural Branch of Russian Academy of Sciences, 91, Pervomaiskaya str., 620108, Ekaterinburg, Russia; ORCID 0009-0004-2807-2222; lab515@ihim.uran.ru

Julia V. Kuznetsova – Institute of Solid State Chemistry of Ural Branch of Russian Academy of Sciences, 91, Pervomaiskaya str., 620108, Ekaterinburg, Russia; ORCID 0000-0002-1253-8727; jukuznetsova@mail.ru

Larisa Yu. Buldakova – Institute of Solid State Chemistry of Ural Branch of Russian Academy of Sciences, 91, Pervomaiskaya str., 620108, Ekaterinburg, Russia; ORCID 0000-0003-3642-7121; buldakova@ihim.uran.ru

Conflict of interest: the authors declare no conflict of interest.